SYSTEM IMPACT OF SILICON CARBIDE POWER DEVICES

BURAK OZPINECI[1,3], LEON M. TOLBERT[1,2], SYED K. ISLAM[1], Md. HASANUZZAMAN[1]

[1]*Department of Electrical and Computer Engineering*
The University of Tennessee, Knoxville, TN 37996-2100

[2]*Oak Ridge National Laboratory*
P.O. Box 2009, Oak Ridge, TN 37831-6472

[3]*Oak Ridge Institute for Science and Education*
Oak Ridge, TN 37831-0117

The emergence of silicon carbide- (SiC-) based power semiconductor switches, with their superior features compared with silicon- (Si-) based switches, has resulted in substantial improvements in the performance of power electronics converter systems. These systems with SiC power devices have the qualities of being more compact, lighter, and more efficient; thus, they are ideal for high voltage power electronics applications such as a hybrid electric vehicle (HEV) traction drive. More research is required to show the impact of SiC devices in power conversion systems. In this study, findings of SiC research at Oak Ridge National Laboratory (ORNL) including SiC device design and system modeling studies, will be given.

1. Introduction

Presently, almost all the power electronics converter systems use silicon- (Si-) based power semiconductor switches. The performance of these switches is approaching the theoretical limits of the Si material. Another material, silicon carbide (SiC), with superior properties compared with Si, is a good candidate to be used in the next generation of power devices.

SiC power devices, with their close-to-ideal characteristics, bring great performance improvements to power converter applications. Some of these advantages compared with Si-based power devices are as follows:

- SiC unipolar devices are thinner, and they have lower on-resistances. At low breakdown voltages (~50V), these devices have specific on-resistances of 1.12μΩ,

around 100 times less than their Si counterparts. At higher breakdown voltages (~5000V), this goes up to 29.5mΩ, 300 times less than comparable devices.[1] With lower R_{on}, SiC power devices have lower conduction losses; therefore, the converters have higher overall efficiency.

- SiC-based power devices have higher breakdown voltages because of their higher electric breakdown field; e.g., Si Schottky diodes are commercially available typically at voltages lower than 300 V, but the first commercial SiC Schottky diodes are already rated at 600 V.
- SiC has a higher thermal conductivity (4.9 W/cm-K for SiC and 1.5 W/cm-K for Si), and SiC power devices have a lower junction-to-case thermal resistance, $R_{th\text{-}jc}$ (0.02 K/W for SiC and 0.06 K/W for Si); thus device temperature increase is slower.
- SiC can operate at high temperatures. SiC device operation at up to 600°C is mentioned in the literature.[2] Si devices, on the other hand, can operate at a maximum junction temperature of only 150°C.
- SiC is extremely radiation hard; i.e. radiation does not degrade the electronic properties of SiC.
- Forward and reverse characteristics of SiC power devices vary only slightly with temperature and time; therefore, they are more reliable.
- SiC-based bipolar devices have excellent reverse recovery characteristics.[3] With less reverse recovery current, the switching losses and EMI are reduced, and there is less or no need for snubbers.
- Because of low switching losses, SiC-based devices can operate at higher frequencies (>20 kHz) not possible with Si-based devices in power levels of more than a few tens of kilowatts.

Although SiC has these advantages compared with Si, the present disadvantages limit its widespread use. Some of these disadvantages are

- Low processing yield because of micropipes. The best wafers available have $<1/cm^2$, but they are more expensive than the typical wafer with $<10/cm^2$.
- High cost–$50 for a 600 V, 4 A Schottky diode (similar Si pn diode <<$1).
- Limited availability (only Schottky diodes at relatively low power are commercially available).
- Need for high temperature packaging techniques that have not yet been developed.

At Oak Ridge National Laboratory (ORNL), a project team consisting of materials, device, and systems researchers in cooperation with The University of Tennessee-Knoxville, Auburn University, and Vanderbilt University are building SiC power MOSFETs. The reason for having a diverse team of people from different disciplines is to develop better devices by encouraging interaction between the researchers who build the devices and the ones who use them. The final power MOSFETs will be used in power electronics converter systems for automotive applications to demonstrate the benefits of SiC-based power devices. One of the selected systems for this project is a traction drive.

2. SiC Devices

2.1 Schottky and pn junction diodes:

The Schottky diode is the least-complex SiC power device. Schottky diodes have been fabricated by forming a metal contact with doped SiC samples. Four different SiC

samples were prepared with characteristics given in Table I. All p-type contacts are Al-Ni, and n-type contacts are Au-As-Ni alloy.

Table I: Characteristics of the SiC samples

Sample	A	B	C	D
Schottky diode (p-type epi)	×	×		
pn diode (p-type epi on n-type substrate)			×	×
Implanted with boron and silicon	×		×	
Implanted with boron only		×		×

The *I-V* plots for samples A and D in Figures 1 and 2 do not show any extra resistance due to the new contact material. This means that Au-As-Ni alloy makes a good contact for n-SiC. Note that based on an extensive literature search, Au-As-Ni contacts are a novel approach for SiC device applications.

Doping densities have been calculated from the slope of the *C-V* characteristic plots. The *C-V* plots for samples A and B are shown in Figures 3 and 4, respectively. The measured values of the activated doping densities are sample A, 5.6×10^{15} cm^{-3}, sample B, 1.02×10^{16} cm^{-3}, sample C, 8.6×10^{17} cm^{-3}, and sample D, 1.3×10^{18} cm^{-3}. These values are similar to the applied doping, another sign of good contact.

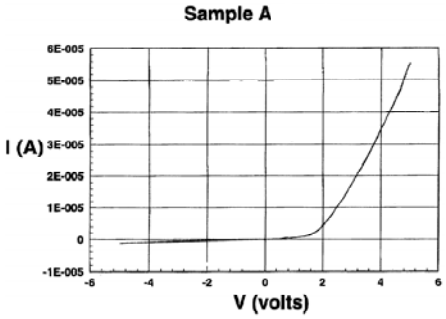

Figure 1. *I-V* Characteristic of sample A.

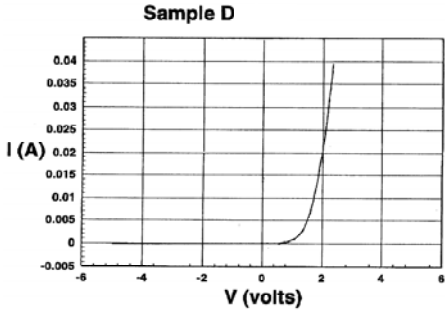

Figure 2. *I-V* Characteristic of sample D.

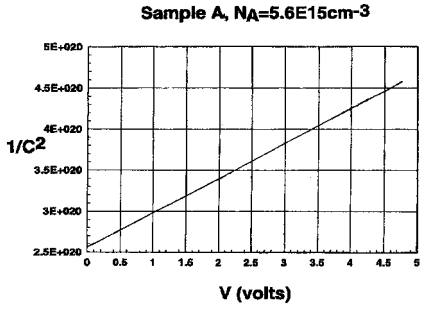

Figure 3. *C-V* plot of sample A.

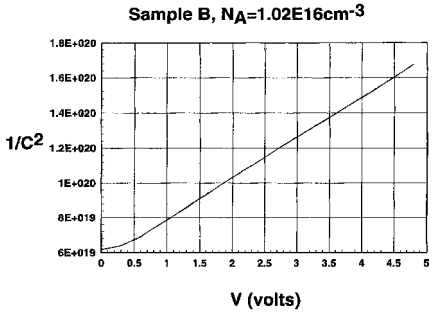

Figure 4. *C-V* plot for sample B.

2.2 MOSFETs:

The double implanted metal-oxide semiconductor (DIMOS) field effect transistor has been frequently used in high-voltage power electronics applications.[4,5] The performance of a DIMOS device is limited by the quasi-saturation behavior in its characteristics. It is shown that such an effect is due to carrier velocity saturation because of the high electric

field, low impurity concentration in the drift layer, and narrow p-body spacing.[6] A detailed study has been made of the vertical DIMOS, and an analytical model has been developed. Figure 5 shows the DIMOS device, identifying different regions of operation. An analytical model is developed from regional analysis of carrier transport in the channel and drift regions. The channel is defined by the compensation between the p-body and n-source lateral diffusion. The current/voltage characteristic in the triode region is given by

$$I_{ch} = \frac{W\mu_{neff}}{2L[1+(\mu_{neff}/2v_{sat}L)V_{ch}]}V_{ch}\left[2C_{ox}(V_{GS}-V_T)-(C_{ox}+C_{do})V_{ch}\right] \quad (1)$$

where W is the width of the transistor, μ_{neff} is the effective electron mobility, v_{sat} is the saturation drift velocity, V_{ch} is the channel voltage, V_{GS} is the gate-source voltage, V_T is the threshold voltage, C_{ox} is the oxide capacitance, and C_{do} is the body depletion capacitance.

The drift region is divided into three parts: an accumulation region A, a drift region B with a varying cross section area, and a drift region C with constant cross section. Voltage across each of these regions is given by

$$V_A = \int_0^{W_j+W_d} E_y dy = \frac{I_D(W_j+W_d)}{W(L_{diff}qN_d\mu_{neff})-I_D/E_C} \quad (2)$$

$$V_B = \frac{I_D}{WqN_d\mu_{neff}\cot\alpha}\log\left[\frac{WqN_d\mu_{neff}(L_{diff}+L_P)-I_D/E_C}{WqN_dL_{diff}\mu_{neff}-I_D/E_C}\right] \quad (3)$$

$$V_C = \frac{I_D(W_t-W_j-W_d-L_P\tan\alpha)}{W(L_{diff}+L_P)qN_d\mu_{neff}-I_D/E_C} \quad (4)$$

where I_D is the drain current and E_c is the critical electric field.

The total drift region voltage $V_{drift} = V_A + V_B + V_C$, and the voltage across the drain to source $V_{DS} = V_{drift} + V_{ch}$. The current/voltage characteristics are shown for the analytical model in Figure 6.

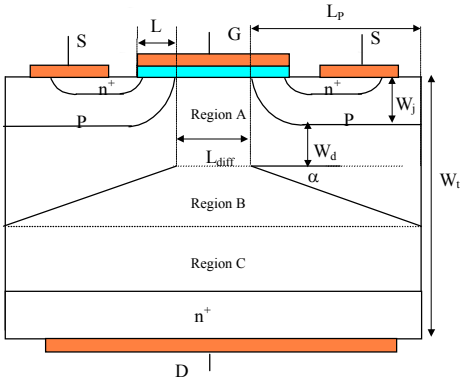

Figure 5. Vertical DIMOS
(Regions A, B, and C form the drift region).

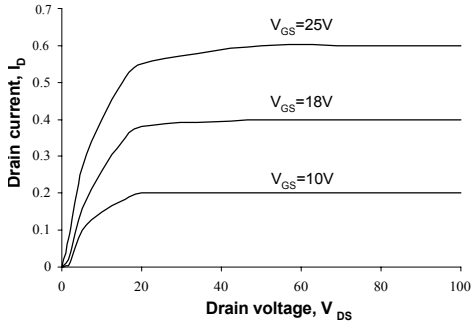

Figure 6. Current-voltage characteristics for DIMOS structure.

3. System Modeling

The main objective of system modeling is to show some of the system-level benefits of using SiC devices in power converter applications, such as the large reduction in the size, weight, and cost of the power conditioning and/or thermal management systems. The selected system for this study is a hybrid electric vehicle (HEV) traction drive. A typical electric traction drive schematic for an HEV is shown in Figure 7. The schematic consists of a battery, a three-phase inverter (dc/ac converter), and an induction motor.

The inverter consists of six MOSFETs and six diodes, two of each on a phase leg. The upper and lower switches on a phase leg turn on and off alternately at frequencies at or below 20kHz with varying duty cycles. The switching instants of the MOSFETs are determined using the popular sinusoidal pulse-width modulation (SPWM) technique. The resulting voltage waveform, v_{ao}, for phase leg A is a chopped waveform with only two values, either $+V_{dc}/2$ or $-V_{dc}/2$, and with as low a harmonic content as possible. The other two phase legs supply similar voltages to the machine, but they are $2\pi/3$ and $4\pi/3$ radians apart from v_{ao}. The induction motor, with its high magnetizing inductance, acts like a filter; thus, the motor currents, unlike the voltages, are sinusoidal.

To evaluate any transportation system, its operation while the vehicle is accelerating, decelerating, stopped, etc., should be considered. For this reason, it is required to simulate the HEV and observe the response of the traction drive over a driving cycle. Using ADVISOR (ADvanced VehIcle SimulatOR), an HEV model is simulated in ADVISOR over the federal urban driving schedule (FUDS), which is a standard 1369 second velocity profile of an average person's vehicle on the way to work.[7]

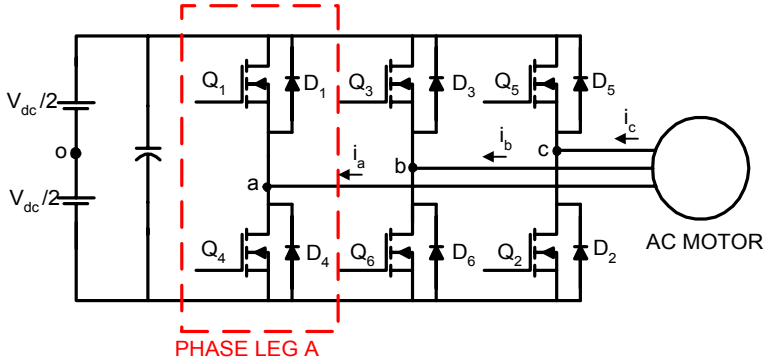

Figure 7. Electric traction drive.

The induction motor in this study is rated at 31 kW, 230 V, 4-pole, 3000 rpm. The peak current passing through the switches is 136 A, and the peak voltage across them is the battery voltage V_{dc}, which is 300 V in this case. Therefore, the MOSFETs and diodes have to be rated at least 400 V and 200 A. The Si MOSFETs are not available in this power range, and SiC MOSFETs are not yet available. For comparison purposes in this study, we will assume that Si MOSFETs exist at high power, too.

The following sections will explain the device loss modeling approach.[8]

4. Diode Modeling

4.1 Conduction losses:

The circuit in Figure 8 is built to find the *I-V* characteristics of the diodes. The dc

voltage supply is varied, and the diode forward voltage and current are measured. This test is carried out at several temperatures up to 250°C.

The results for both Si pn and SiC Schottky diodes are given in Figure 9, in which it can be seen that the forward voltage of the SiC diode is higher than that of the Si diode. This is expected because of SiC's wider bandgap. Another difference between these two diodes is their high-temperature behavior. As the temperature increases, the forward characteristics of the Si diode change severely while those of the SiC diode stay confined to a narrow region. Note that the pn diode (negative) and the Schottky diode (positive) have different polarity temperature coefficients; that is why the slope of the curve at higher currents is increasing in the Si diode case and decreasing in the SiC diode case with the temperature increase.

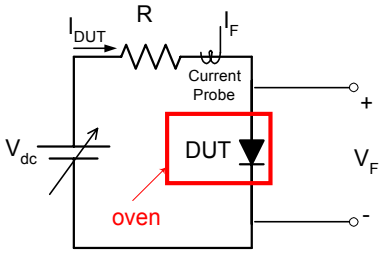

Figure 8. *I-V* characterization circuit.

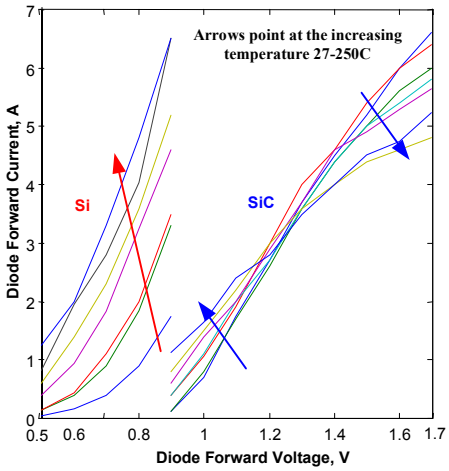

Figure 9. Experimental *I-V* characteristics of the Si and SiC diodes in an operating temperature range of 27 C to 250°C.

For the traction drive application, the forward characteristics of 200 A rated diodes are required. Assume that the 200 A diode is equivalent to twenty 10 A diodes connected in parallel. Then, in the *I-V* characteristics of the resulting diode, I_s and R_s should be changed accordingly.

The diode equation is

$$I = I_S \left(e^{q\left(V - IR_S\right)/nkT} - 1 \right). \tag{5}$$

I_s is directly and R_s is inversely proportional to the area of the device. For the 200 A diode, the area is increased 20 times; therefore, I_s increases 20 times and R_s decreases 20 times. The resulting diode equation is

$$I = 20 \times I_S \left(e^{q\left(V - I\frac{R_S}{20}\right)/nkT} - 1 \right). \tag{6}$$

If a line is drawn along the linear high-current portion of the *I-V* curves of (6) extending to the x-axis, the intercept on the x-axis is V_D and the slope of this line is $1/R_D$.

After these parameters are obtained for each diode at different operation temperatures, the conduction losses can be calculated using (7).[8]

$$P_{cond,D} = I^2 \cdot R_D \cdot \left(\frac{1}{8} - \frac{1}{3\pi} M \cos\phi\right) + I \cdot V_D \cdot \left(\frac{1}{2\pi} - \frac{1}{8} M \cos\phi\right). \quad (7)$$

where M is the modulation index and ϕ is the power factor.

The conduction losses for an SiC diode and for an Si diode are plotted in Figures 10 and 11, respectively. These plots show that for low temperatures (T < 55°C), the conduction loss of the SiC diode is less than that of the Si diode, and vice versa for higher temperatures (T < 55°C). This is because the series resistance of the Schottky diode is increasing while that of the pn diode is decreasing. This increase seems to be a disadvantage in the SiC Schottky diode case; however, note that the Si diode cannot withstand temperatures over 150°C.

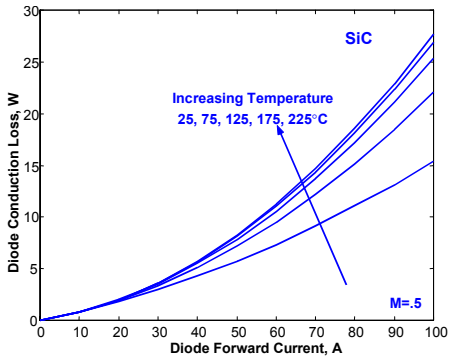

Figure 10. Conduction losses for a 200A SiC diode.

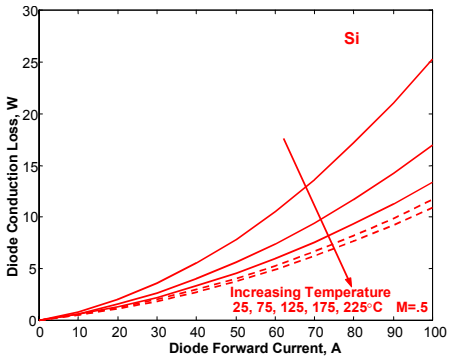

Figure 11. Conduction losses for a 200A Si diode.

4.2. Switching losses:

The most important part of the diode switching loss is the reverse recovery loss. The rest of the losses are negligible. Reverse recovery losses, in this paper, will be calculated experimentally.

For this purpose, the chopper circuit in Figure 12 was built. Here, the main switch Q is turned on and off at 1 kHz with a duty ratio of 75%. When Q is on, the diode D is off, and the current is forced by the dc supply to build up through the load and Q. When Q turns off, the load current starts flowing through D and the load. In this mode, the dc supply is out of the loop, and therefore the current starts decreasing. After a while, Q is turned on again and then D turns off. The typical diode turn-off waveforms are given in Figure 13. These experimental waveforms show that the Si diode switching losses are almost three times more than those of the SiC diode.

The peak reverse recovery current, I_R, and the switching loss, P_{sw}, of the diodes are measured at different operating temperatures with varying load currents. The results are plotted in Figures 14 and 15. In Figure 14, I_R of the Si diode is higher than that of the SiC diode at any operating temperature. As the temperature increases, the difference increases because the I_R of the Si diode increases with temperature, but that of the SiC diode stays constant. Note that the Si diode failed when operating at 150°C and 4.5 A while the SiC diode survived that temperature and failed at a higher 250°C and 4 A.

To obtain a 200 A diode model for the traction drive, assume as before that 20 of the

diodes tested here are connected in parallel to form a 200 A diode. The switching losses multiplied by 20 give the switching losses of the 200 A Si and SiC diodes (Figure 15).

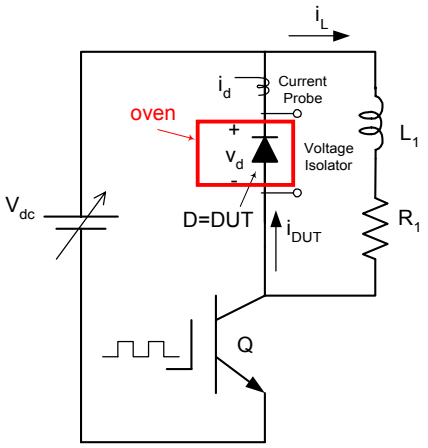

Figure 12. Reverse recovery loss measurement circuit.

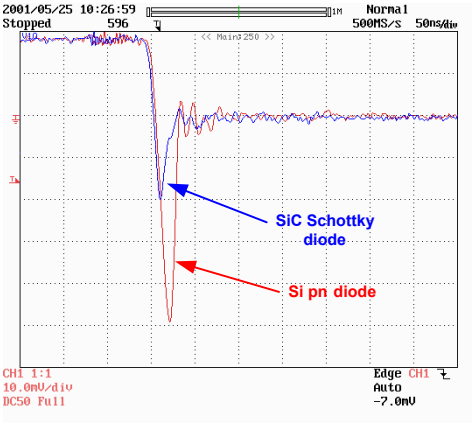

Figure 13. Typical reverse recovery waveforms of the Si pn and SiC Schottky diode (2 A/div.).

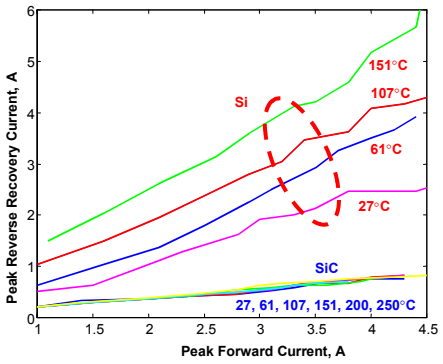

Figure 14. Peak reverse recovery values with respect to the forward current at different operating temperatures.

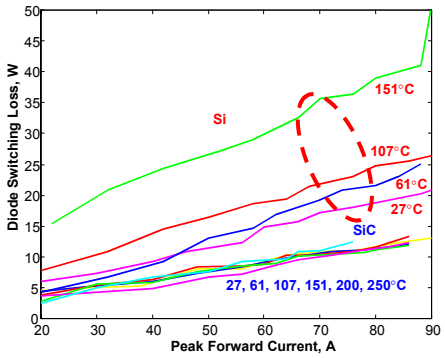

Figure 15. Diode switching loss of 200A diode at different operating temperatures.

5. Results

The HEV traction drive is simulated over the FUDS cycle using the model developed in the previous sections. The loss profiles of a diode and a MOSFET in the drive are shown in Figure 16. SiC diode losses are lower than Si diode losses mostly because the SiC diode has lower reverse recovery losses. On the other hand, SiC MOSFET losses are lower because the switching losses are similar but SiC MOSFET conduction losses are lower. The reason for lower conduction losses is the lower specific on-resistance [$R_{on,sp}$ (Si) = 180×10^{-3} Ω-cm^2, $R_{on,sp}$ (SiC) = 0.3×10^{-3} Ω-cm^2].[1]

Total energy loss (six diodes and six MOSFETs) is 925 W·s for the Si inverter and 338 W·s for the SiC inverter over the FUDS cycle. The corresponding efficiency of the Si inverter is 80–85%, while that of the SiC inverter is 90–95%. This is a 10% increase in

the average efficiency. As a result, the battery in the HEV with the SiC inverter will need less charging than the one with the Si inverter.

The loss profiles in Figure 16 are fed to the thermal models of the devices. The resulting junction temperature profiles are shown in Figure 17. Natural air-cooled heatsinks are used to limit the junction temperature to 150°C for Si and 175°C for SiC. The latter temperature limit is found on the datasheet of the Infineon SiC Schottky diode used in this study.[9] The resulting heatsink volumes and masses for each device and each inverter are given in Table II. Using SiC devices instead of their Si counterparts in an HEV traction drive reduces the size and weight of the heatsink to one-third. Note that a heatsink usually occupies one-third the volume of the converter and weighs more than the electronics.

Theoretically, SiC devices can work at higher temperatures. If new packaging techniques are developed such that these higher temperatures could be used as the junction temperature limits, then the amount of cooling required would be less, and more weight and volume savings would be possible.

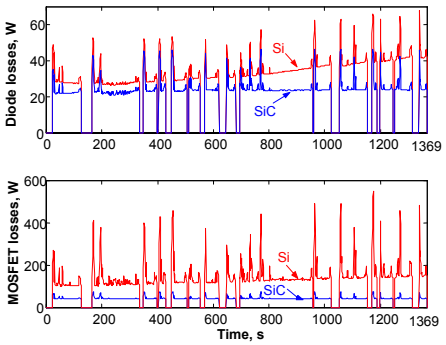

Figure 16. Total loss profile for a diode (top) and a MOSFET (bottom).

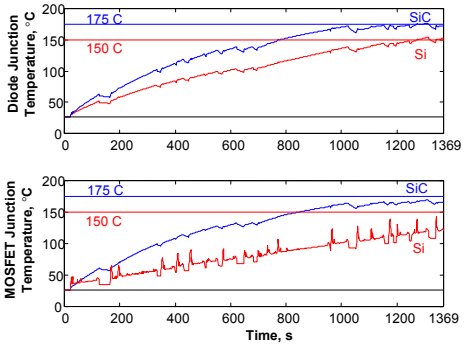

Figure 17. Junction temperature profiles of the diodes and MOSFETs in the three-phase inverter.

Table II: Heatsink mass and volume for each device and inverter

	Volume (cm^3)	Mass (g)
Si diodes	444	1200
SiC diodes	162	450
Si MOSFETs	1554	4200
SiC MOSFETs	444	1200
Si inverter	***1998***	***5400***
SiC inverter	***606***	***1650***

6. Conclusions

Even the first SiC devices show the superiority of SiC compared with Si. One of the challenges for building SiC power devices is the contact material. In this paper a new contact material, Au-As-Ni alloy, is introduced. The *I-V* characteristics of the SiC Schottky diodes built with this contact material show that it makes solid and reliable contact with SiC.

System studies show that power electronics systems using SiC power devices are on average 10% more efficient because of the low losses of the SiC power devices. Moreover, with their high-temperature operation capability, they need less stringent cooling requirements. In the HEV traction drive studied here, using SiC power devices saves 1392cm^3 of space and 3.75kg of weight are saved.

The weight reduction and efficiency increase result in an increase in the fuel economy of the vehicle and longer lifetime for the battery.

Note that SiC technology is still in its infancy. More studies like the one in this paper are required to forecast the impact of SiC power devices. When this technology matures, for power devices in the medium-to-high power range, the future will be SiC.

Acknowledgements

This project is supported by ORNL and the U.S. Department of Energy's Office of Transportation Technology Freedom Car Research Program.

The authors would like to thank Michael Krach and Michael Brandt from Infineon Technologies AG for supplying the SiC Schottky diode samples, and Mustafa Saglam from the Technical University of Darmstadt for contacting them about the samples. The authors also would like to thank Dr. O. W. Holland of ORNL for providing SiC samples and Dr. F.C. Jain of the University of Connecticut for providing facilities and assistance for material processing, fabrication, and testing of SiC diodes.

The submitted manuscript has been authored by a contractor of the U.S. Government under Contract No. DE-AC05-00OR22725. Accordingly, the U.S. Government retains a non-exclusive, royalty-free license to publish from the contribution, or allow the others to do so, for U.S. Government purposes.

References

1. M. Bhatnagar and B. J. Baliga, "Comparison of 6H-SiC, 3C-SiC, and Si for power devices," *IEEE Trans. on Electron Devices*, 40 (3), pp. 645–655, March 1993.
2. K. Shenai, R. S. Scott, and B. J. Baliga, "Optimum semiconductors for high–power electronics," *IEEE Transactions on Electron Devices*, 43 (9), pp. 1811–1823, Sept. 1989.
3. A. Elasser, M. Kheraluwala, M. Ghezzo, R. Steigerwald, N. Krishnamurthy, J. Kretchmer, and T. P. Chow, "A comparative evaluation of new silicon carbide diodes and state-of-the-art silicon diodes for power electronic applications," *IEEE IAS Annual Meeting Conference Proceedings*, pp. 341–345, 1999.
4. B. J. Baliga, *Modern Power Devices*, Wiley, New York, 1987.
5. D. A. Grant and J. Gower, *Power MOSFETs: Theory and Application*, Wiley, New York, 1989.
6. M. Darwish, "Study of the quasi-saturation effect in VDMOS transistors", *IEEE Transactions on Electron Devices*, vol. ED-33, no. 11, pp. 1710–1716, 1986.
7. http://www.ctts.nrel.gov/analysis/advisor.html
8. B. Ozpineci, L. M. Tolbert, S. K. Islam, and Md. Hasanuzzaman, "Effects of silicon carbide (SiC) power devices on PWM inverter losses," *The Annual Conference of the IEEE Industrial Electronics Society (IECON'01)*, pp. 1187–1192, 2001.
9. http://www.infineon.com/cgi/ecrm.dll/ecrm/scripts/prod_cat.jsp?oid=-8681